ATTRIBUTES OF Q&T DUCTILE IRON WITH NOVEL MICROSTRUCTURES

Richard B. Gundlach and John M. Tartaglia (ID)
Element Materials Technology, Wixom, MI, USA

Abstract

A novel approach to austenite grain refinement was applied to quench and temper ductile iron in order to improve the tensile properties. Castings of two ductile iron alloys were intercritically (IC) austenitized near the upper critical temperature to produce a fine-grained lamellar austenite-ferrite structure and were subsequently quenched and tempered. The lamellar austenite + ferrite formed in the dendrite core region without forming a continuous network of austenite in the interdendritic regions. The austenite grain size was substantially finer than the polygonal austenite grain structure produced by conventional hardening above the critical temperature. In contrast to earlier researchers of IC austenitized DI who produced more ferrite by austenitizing at lower IC temperatures, the present study achieved higher austenite fractions and thus greater lamellar martensite contents after quenching. On tempering up to 540 °C (1000 °F), the supercritically heat-treated martensitic structures produced secondary graphite, whereas none was observed in the intercritically heat-treated materials. Differing upper critical temperatures and manganese and silicon contents were measured in the core and interdendritic regions for one of the as-cast irons. The resulting properties of the lamellar martensite and ferrite microstructure were determined and compared to those of conventional quench and tempered ductile iron with a fully martensitic microstructure. When the properties are compared to the minimum specifications for the Q&T grades of ASTM A536 Grade 120-90-02 and ISO 1083 Grade 900-2, the intercritically austenitized alloys exhibited the specified tensile properties with high ductility.

Keywords: ductile iron, intercritical heat treatment, mechanical properties, quench and temper martensite, grain refinement

Introduction

Grain refinement is quite effective in increasing the strength of metals. For wrought and cast steels, refinement of the prior austenite grain structure improves the ductility and toughness of the quenched and tempered properties.[1–5] The traditional methods of grain refinement include mechanical deformation and/or micro-alloying to restrict grain growth with nitride and carbide precipitates. Currently, methods used to refine grain size and control grain growth during the austenitization of ductile iron castings are not practiced or available.

The present authors are proposing a novel approach to refining austenite grain size in ductile iron. Ductile iron has a unique microstructure that allows it to develop unusual

transformation structures, due to the fact that the graphite is relatively isolated from the iron matrix. This isolation of the carbon phase affects the nature of phase transformation in heat treatment. On heating above the lower critical temperature (intercritical austenitizing), a lamellar structure can form with alternating layers of austenite and ferrite. Compared to the coarse-grained, polygonal austenite that forms on heating above the upper critical temperature, the lamellar austenite structures can be an order of magnitude finer. This lamellar structure forms in packets within the ferrite grains, as shown in Figure 1a.

Several researchers[6–15] have investigated intercritical (IC) heat treatment of ductile iron (DI) to take advantage of the fine-grained acicular austenite in ferrite structure. When quenched from the intercritical temperature, the acicular structure is preserved, i.e., the acicular austenite transforms to martensite and the as-quenched microstructure displays the same acicular morphology that developed at the

intercritical temperature. Likewise, when austempered from the IC temperature, ausferrite can form and the ausferrite-ferrite structures can exhibit high strength and ductility.[12,13] When cooled in air, the acicular austenite transforms to pearlite and the microstructure consists of acicular pearlite in ferrite which also exhibits high strength and ductility.[10,11,14]

Most previous work was performed with intercritical austenitizing near the middle of the intercritical temperature range. Also, many earlier investigators did not ferritize prior to austenitizing, so they heat-treated mixed ferrite and pearlite structures. Consequently, they did not achieve a fully lamellar austenite in ferrite microstructure with high austenite fraction. Figure 1b from our earlier work[11] is similar to the prior work of other investigators where
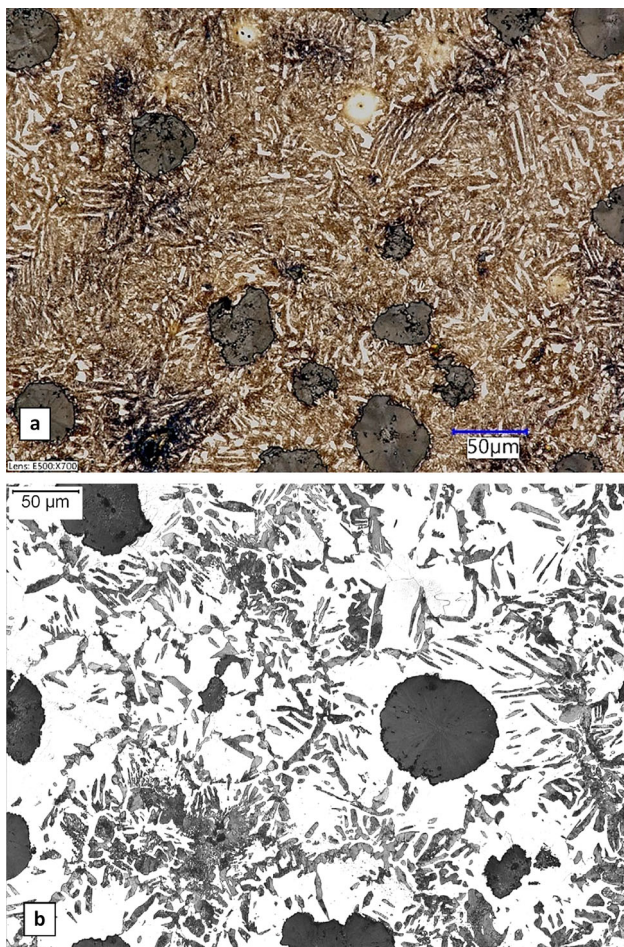

Figure 1. Optical micrographs of quenched microstructure illustrating the unique lamellar austenite in ferrite structure that formed by intercritical heat treatment. (a) Packets of lamellar martensite and ferrite form when this ductile iron sample was quenched and tempered after austenitizing near the upper critical intercritical temperature. (b) This sample was intercritically austenitized near the middle of the intercritical temperature range; it produced isolated acicular needles in a largely ferritic matrix.[11] Etched in 2% Nital.

intercritical heat treatment produced isolated acicular martensite needles in a largely ferritic matrix.

This novel approach to austenite grain refinement was applied to quench and temper ductile iron in order to improve the tensile properties, i.e., the strength-ductility balance. In this study, ductile iron having a fine-grained lamellar austenite-ferrite structure was quenched from an intercritical temperature and tempered. The resulting mechanical properties of the lamellar martensite and ferrite structure were compared with the specifications for Q&T grade 120-90-02 of ASTM A536 and grade 900-2 of ISO 1083.[16,17]

Background Information

In typical cast iron alloys that contain significant amounts of silicon, the eutectoid transformation region contains a three-phase field where austenite, ferrite and graphite co-exist. The three-phase region is shown schematically in
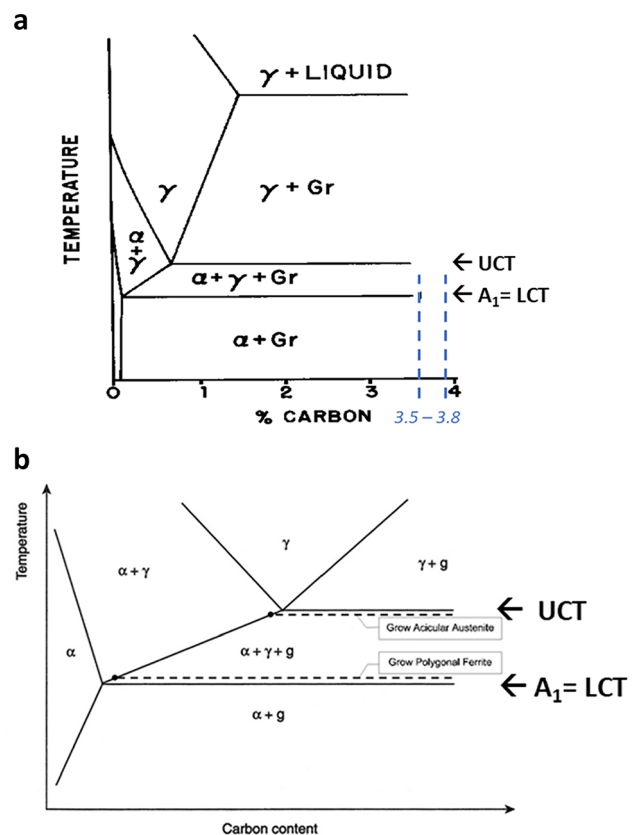

Figure 2. These schematics of Fe-2.4Si-C phase diagram for DI illustrate the three-phase field between the lower critical temperature (LCT and A1) and the upper critical temperature (UCT). (a) The typical carbon range of 3.5 to 3.8%C for DI is delineated. (b) The difference between IC austenitizing near the upper critical temperature (where mostly austenite) is formed, like the present study, and IC austenitizing near the LCT (where significant ferrite is formed) like many earlier studies is differentiated.[18]

Figure 2 for a typical ductile iron Fe-Si-C alloy. These schematics represent an idealized portion of the Fe-2.4%Si-C phase diagram section in the original publication.[18] The region is defined by the lower critical temperature (LCT) or A_1, below which the equilibrium structure is ferrite + graphite. Upon heating above the LCT, austenite begins to form, and the volume fraction of austenite increases with temperature. When exceeding the upper critical temperature (UCT) the remaining ferrite disappears and the metallic matrix is fully austenitic. In typical ductile iron chemistries, the LCT and UCT are separated by 67 to 89 °C (120 to 160 °F).

While heating in the intercritical region, the metallic matrix is partially austenitized by recarburization of the matrix. The authors hypothesize that recarburization of the matrix occurs by diffusion of carbon from the graphite nodule along the ferrite grain boundaries that intersect the graphite nodule. Subsequently, carbon at the grain boundaries diffuses into the ferrite matrix along intercrystalline planes to produce acicular grains of austenite within the ferrite grain. Once equilibrium is reached, the resulting microstructure consists of numerous acicular austenite grains surrounded by the parent ferrite which, at the intercritical temperature, is stable and in equilibrium with the austenite phase.

At temperatures near the upper critical temperature, the austenite fraction is high as shown in Figure 2b and the acicular structure is well developed, as illustrated in the oil-quenched sample in Figure 3a. Alternatively, with air-cooling, the acicular austenite that formed at the intercritical temperature transforms to pearlite with the same acicular morphology, resulting in a similar fine-grained structure consisting of acicular pearlite in ferrite, as shown in Figure 3b.

Experimental Procedures and Results

Materials

The experimental work focused on two ductile iron alloys with aim chemistries containing nominally 2.4%Si, 0.3%Mn, 0.6%Cu and either 0.2 or 1.2%Ni. Except for the somewhat elevated Ni (0.24%), Alloy 1 is typical and representative of Grade 700/2 (30-60mm sections) of ISO 1083. The Y-block castings poured for this study generally conformed to the 3-inch (75-mm) Y-block design of ASTM A536 specification, except that the Y-block was extended to 191 mm (7.5 in.) in length. Figure 4 shows a schematic of the castings and the rest of the casting details are contained in references 14 and 15.

Table 1 lists the compositions for the two induction-melted alloys. Nickel was added for hardenability and to reduce the segregation network, by attempting to bring the
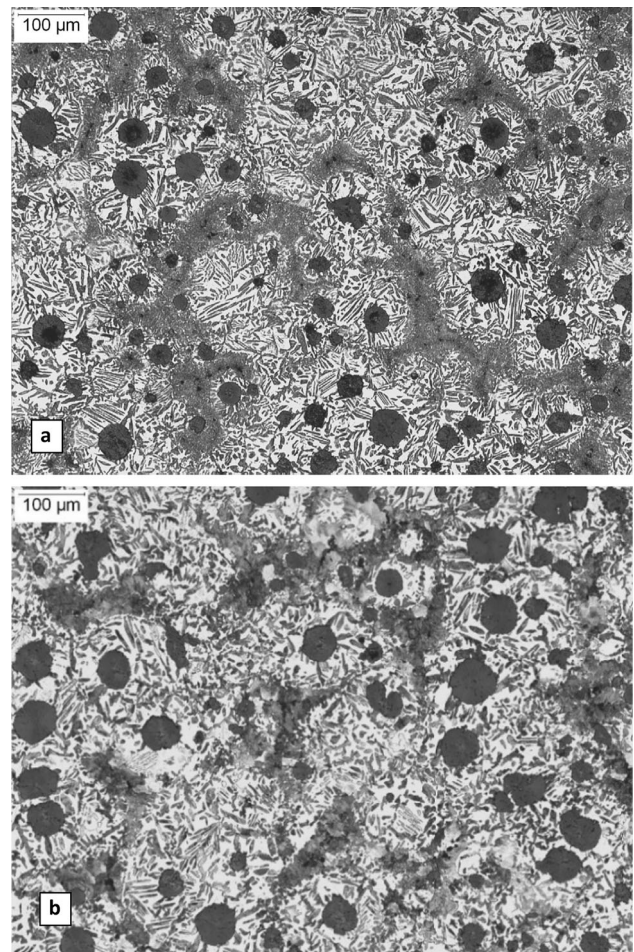

Figure 3. Optical micrographs are shown for ductile iron that was (a) oil-quenched (with ferrite and martensite) and (b) air-cooled (with ferrite and pearlite) after intercritically austenitizing.[10] Etched in 2% Nital.
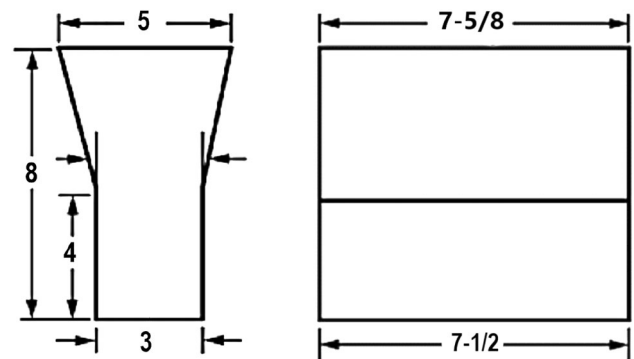

Figure 4. Modified 75-mm (3-inch) Y-block used in experimental ductile iron heats. (All dimensions in inches.)[14,15]

intercritical temperatures of the dendritic core and interdendritic regions closer together.

Figure 5 shows a schematic where various samples were obtained for the study.

Table 1. Compositions for Two Experimental Alloys, in wt-%

Element	Alloy 1	Alloy 3	Method**
CE*	4.40	4.37	Calc
C	3.59	3.46	L
S	0.015	0.016	L
P	0.032	0.035	GDS
Si	2.34	2.42	GDS
Mn	0.30	0.29	GDS
Cu	0.61	0.59	GDS
Ni	0.24	1.15	GDS
Cr	0.09	0.09	GDS
Mo	<0.01	<0.01	GDS
V	<0.005	<0.005	GDS
Al	0.009	0.010	GDS
Ti	0.005	0.006	GDS
Sb	<0.005	<0.005	GDS
Sn	<0.005	<0.005	GDS
Mg	0.044	0.053	GDS
Ce	0.015	0.016	GDS

*CE = %C + (%Si + %P)/3 + %Ni/12

**Calc = Calculated; L = Leco combustion method; GDS = Glow Discharge Spectrometry
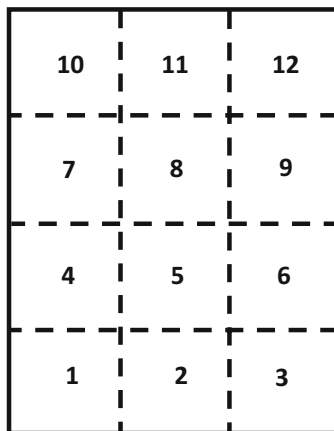
Test Bar Locations

Heat Treatment Coupons: #5 & 8

Heat Treated Tensile Bars: #1, 2 and 3

Figure 5. This schematic shows the sampling of the Y-block casting test coupon and identifies the test locations.[14,15]

The microstructures were evaluated for each heat by excising samples from a location 50 mm (2 in.) away from one end of the Y-block test section and at a position 25 mm (1 in.) up and 25 mm (1 in.) inwards from the bottom edge. All samples were compression-mounted in Bakelite, then
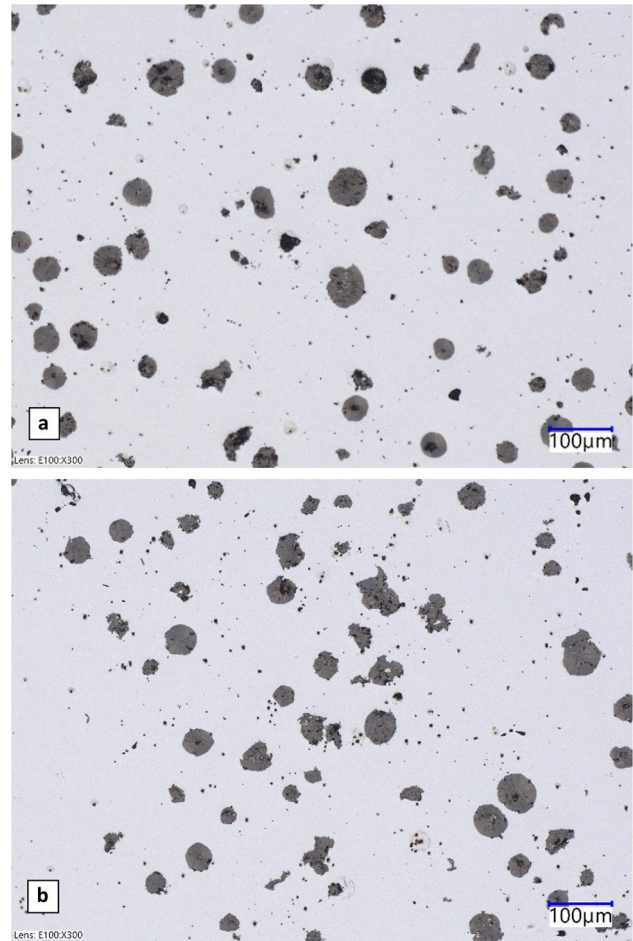

Figure 6. Optical micrographs showing the graphite structures of the two experimental alloys are shown for (a) Alloy 1 and (b) Alloy 3. As-Polished.

ground, polished, and Nital-etched in accordance with ASTM E3-11(2017).

The graphite structures of the two alloys are shown in Figure 6.

In the as-cast condition, all castings were nearly fully (>90%) pearlitic. A representative micrograph of the etched structure of Alloy 3 (Heat 3) is shown in Figure 7.

Nodularity was determined by image analysis using compactness (>0.7) as the shape factor in accordance with ASTM A247-19. Graphite particles less than 10 μm were ignored. Nodule count was determined by image analysis in accordance with E1245-03(2016). The image analysis results are shown in Table 2.

Heat Treatment Approach

Initially, experimental heat treatments were conducted on samples in the two locations shown in Figure 5, to study the
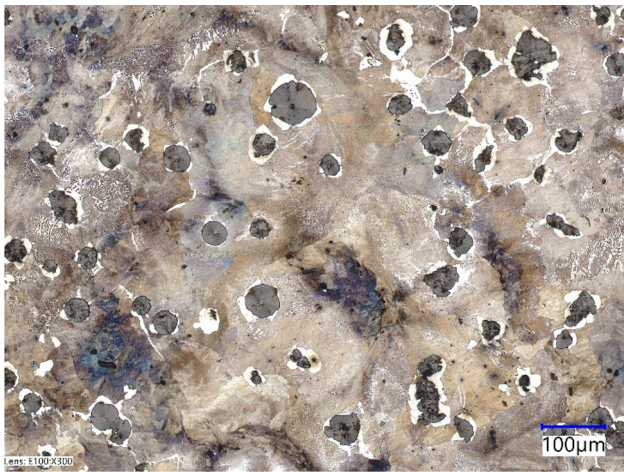
Figure 7. Optical micrograph of the pearlite microstructure of Alloy 3 in the as-cast condition. Etched in 2% Nital.

Table 2. Microstructure Ratings for Two Experimental Alloys

Parameter	Alloy 1	Alloy 3
Nodularity,%	93	91
Nodule Count, nodules/mm^2	45	32
Average Nodule Size, μm	38	49
Maximum Nodule Size, μm	282	231
Ferrite Content, %	5	10

heat treatment response as discussed in references 14 and 15. To maximize strength, the acicular austenite component of the IC heat-treated microstructure should be maximized. Consequently, the casting must be heated as close to the upper critical temperature as possible without losing the fine-grained acicular austenite structure. That is, without incurring grain growth, where the fine-grained acicular austenite + ferrite is replaced by coarse-grained polygonal austenite (with no ferrite).

Therefore, the upper critical temperature is particularly important in determining the optimum intercritical heat treatment cycle for the alloys. Researchers[19] have determined the upper and lower critical temperatures for ductile iron as a function of chemical composition, and these formulae were used to calculate the UCT and LCT temperatures of the two experimental alloys. More recently,[14] experiments were conducted on these alloys to determine the optimum intercritical heat treatment temperature. They showed that the acicular austenite + ferrite structure persisted well above the calculated UCT temperature; this is why the present authors conducted all intercritical heat treatments at 11 °C (20 °F) above the calculated UCT, which the authors believe underestimates the true UCT, especially in the dendrite core. Therefore, the calculated

UCT temperatures were used for guidance only. When heating above the UCT, ferrite disappears, first in the interdendritic regions and eventually in the core microstructure. Note that due to alloy segregation, the UCT of the interdendritic region is lower than that of the dendrite core, as discussed later in this paper.

In reference 14, the heat treatment response of a 3.5C-2.4Si-0.3Mn-0.6Cu-0.5Ni alloy was investigated. Samples were heat-treated just below the UCT and quenched after 0, ¼, 1 and 2 hours. At shorter times, more ferrite and less martensite were obtained. Equilibrium was achieved between 1 and 2 hours. This long time required for the ferritic-austenitic structures to reach equilibrium is consistent with the results of earlier work.[20]

As temperature approaches the UCT, the austenitic network in the interdendritic regions thickens and becomes more continuous. Furthermore, the dendritic core shrinks and becomes less continuous. Eventually, the austenite grain size increases due to grain growth. This change in the structure in the interdendritic regions is illustrated in Figure 8 for a similar ductile iron alloy from Ref 14 when heated and quenched from three temperatures between 811 and 832 °C (1491 and 1531 °F), respectively.

At some point, the interdendritic zones will become thicker and more continuous, and ductility will suffer. Consequently, it was decided that the best properties will be obtained when the ferrite fraction is low (as shown by the upper dashed line in the bottom of Figure 2) and yet, the interdendritic network is still discontinuous. Therefore, all intercritical heat treatments were conducted at UCT + 11 °C (20 °F).

Since the desired lamellar austenite structure only forms in ferrite, to achieve a uniform acicular structure throughout, it was necessary to eliminate pearlite. Consequently, ferritizing was performed by subcritical annealing prior to IC heat treatment. In initial experiments, test pieces were annealed to attain a fully ferritic structure. Subsequently, subcritical annealing was performed on heating to the intercritical temperature.

Austenitizing

A summary of the heat treatment parameters used in the intercritical heat treatment of the test bars of each alloy are shown in Table 3. The tensile test blanks, which measured 25 by 32 by 190 mm (1 by 1-1/4 by 7.5 in.), were cut from the bottom of the Y-block legs of each alloy in the three locations shown in Figure 5. When heating the test samples, extra care was taken to adjust the PID parameters to avoid heating too fast and "overshooting" the setpoint temperature.
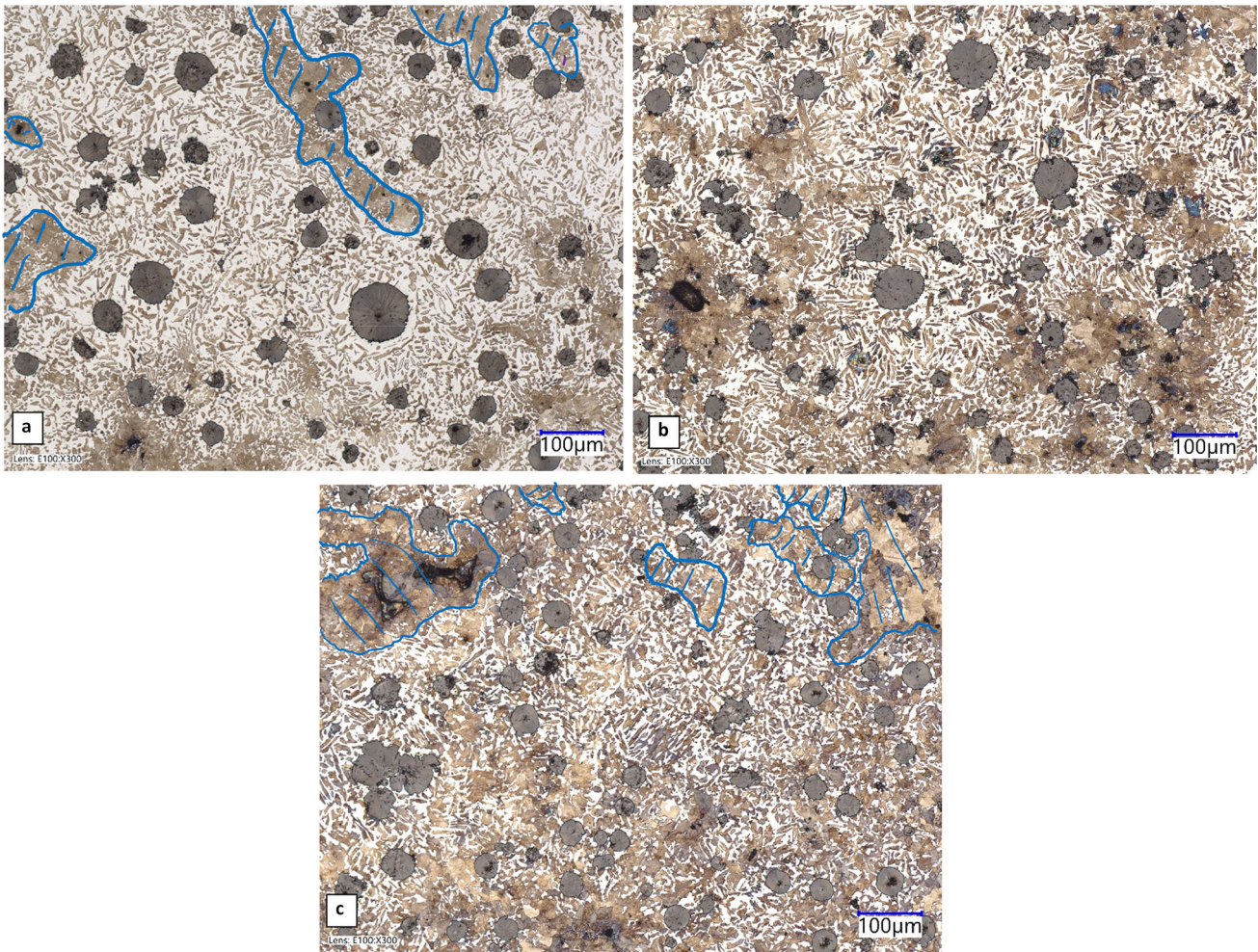
Figure 8. *Optical micrographs illustrating the increase in continuity of the interdendritic network with intercritical austenitizing temperature upon quenching of a 3.5C-2.4Si-0.3Mn-0.6Cu-0.5Ni alloy from (a) 811 °C (1491 °F), (b) 822 °C (1511 °F), and (c) 833 °C (1531 °F).[14] These three temperatures are still below the actual UCT for the dendrite core because ferrite is still visible there. Selected interdendritic regions are outlined in blue in Figures 8a and 8c. The regions containing significant white contrast in Figure 8a are largely ferrite and correspond to the dendritic core regions. Etched in 2% Nital.*

Tempering

A tempering study was conducted to determine the optimum tempering temperature in order to obtain tensile properties comparable to ASTM A536 Grade 120-90-02, the common Q&T grade of that specification. Based on published data,[21] it was decided that to obtain a strength of 120 ksi (900 MPa) a hardness between 250 and 300 HB is needed and that the tempering response of the intercritically heat-treated material must be determined. Tempering of small heat-treated samples was conducted between 482 and 567 °C (900 and 1050 °F) for 2, 4 and 8 hours.

After tempering, the samples were ground to make the surface clean, smooth and flat. Hardness testing was conducted in accordance with ASTM E10-18 using a 10-mm tungsten carbide ball and 3000-kg load. The test results indicated that tempering at 540 °C (1000 °F) would produce the desired hardness (280 HB), and the test blanks of each alloy were heat-treated accordingly. Both supercritically and intercritically austenitized samples were tempered and tested.

Mechanical Testing

After all heat treatments were completed, the test blanks were sectioned and machined to obtain tensile specimens. Initially, Brinell hardness was determined on the test blanks after grinding to make the surface clean, smooth and flat. The testing was conducted in accordance with ASTM E10-18.

Table 3. Parameters for Intercritical (IC) Austenitizing Heat Treatment

Step	Description	Reason	Heating Rate °C/h (°F/h)	Aim Temperature °C (°F)	Time hours
1	First heating rate	Typical heating rate for castings	111 (200)	649 (1200)	5
2	Second heating rate	Slow heating rate for better temperature control to avoid overheating	56 (100)	732 (1350)	1.5
3	Ferritize	Convert all pearlite to ferrite		732 (1350)	2
4	Third heating rate	Slow heating rate for better temperature control to avoid overheating	28 (50)		≈3.5
5	"Intercritically" (IC) austenitize at 11°C (22°F) above the *calculated* UCT*	Ferrite still exists above the *calculated* UCT and long times simulate commercial heat treatment		Alloy 1: 832 (1530)	4
				Alloy 3: 827 (1520)	
6	Quench in oil	Required to form martensite in all alloys and avoid quench cracking			

*The calculated lower (LCT) and upper (UCT) critical temperatures for alloy 1 are 753 and 821°C (1388 and 1510F°) and for alloy 3 are 752 and 816°C (1385 and 1501°F), respectively.[19]

Table 4. Standard Tensile Properties and Hardness of the Q&T Test Bars

Austenitizing treatment*	Alloy	Tempering temperature & time °C (°F)/h	Brinell hardness HB	0.2% Offset yield strength (YS) MPa (ksi)	Ultimate tensile strength (UTS) MPa (ksi)	Elongation (El) %	Reduction of Area (RA) %
Intercritical	1	538(1000)/4	280	669 (97.0)	860 (125)	5.2	5.6
				650 (94.3)	839 (122)	4.4	5.0
	3	538(1000)/4	287	678 (98.4)	860 (125)	5.2	4.5
				663 (96.1)	746 (108)**	1.1**/**	1.7**
Supercritical	1	538 (1000)/8	283	727 (105)	871 (126)	3.5	2.8
				732 (106)	883 (128)	4.1	3.9
	3	538 (1000)/8	294	790 (115)	946 (137)	4.0	3.9
				785 (114)	870 (126)	1.4	2.8
ISO 1083 Minimum Specifications for Grade 900-2				600 (—)	900 (—)	2	–
ASTM A536 Minimum Specifications for Grade 120-90-02				— (90)	— (120)	2	–

*Austenitizing temperatures and times are shown in Table 3.

**Optical examination of this fracture surface revealed a few large degenerate graphite inclusions. These inclusions are considered responsible for the low tensile strength and ductility values.

Duplicate round tensile bars were machined from each test blank. All tensile specimens were machined with a standard 9 mm (0.35 in.) diameter by 36 mm (1.4 in.) long gauge section and with threaded grip ends. Tensile properties were determined in accordance with ASTM E8-21. Tensile toughness U_T (in units of MPa-mm/mm or ksi-in./ in.) is related to the area under the stress–strain curve, as approximated[22] for a ductile material by the following formula:

$$U_T = 1/2 * (YS + UTS) * El \qquad \text{Eqn. 1}$$

The results of mechanical testing of the heat-treated materials are shown in Tables 4 and 5.

When compared at equivalent tempering temperatures, the intercritically (IC) austenitized materials had somewhat lower strengths, higher ductility, and higher toughness than the supercritically (SC) austenitized materials. The combination of yield strength and tensile elongation is substantially above the ISO 1083 Grade 900-2 properties for sections of <30 mm (<1.2 in.). The properties also exceeded the minimum properties for ASTM A536 Grade 120-90-02.

Figure 9 shows a correlation of strength with hardness for the IC heat-treated materials, including linear regression equations and associated coefficients of determination (r^2

Table 5. Tensile Toughness of the Q&T Test Bars

Austenitizing treatment*	Alloy	Tempering temperature & Time °C (°F)/h	Toughness (U_T)	
			MPa-mm/mm	ksi-in./in.
Intercritical	1	538(1000)/4	39.8	5.77
			32.8	4.76
	3	538(1000)/4	40.0	5.81
			7.7**	1.12**
Supercritical	1	538 (1000)/8	28.0	4.04
			33.1	4.80
	3	538 (1000)/8	34.7	5.04
			11.6	1.68

*Austenitizing temperatures and times are shown in Table 3.

**Optical examination of this fracture surface revealed a few large degenerate graphite inclusions. These inclusions are considered responsible for the low toughness values.

values) for the Q&T materials of this study and the normalized materials from a previous study.[11] In general, tensile strength increased with hardness in a linear manner. After including the Q&T materials of this study, the correlation between hardness and tensile strength was extended to higher strengths. However, due to the microstructure change from pearlite to martensite as IC normalizing is compared to IC Q&T, as shown by the superimposed dashed blue box, the yield strength for the Q&T materials is well above the dashed extension of the YS versus hardness line for the normalized materials.

Statistical Testing

Microsoft Excel® was used to obtain summary statistics for selected mechanical properties. In this case, two sets of data in Tables 4 and 5 were separated by austenitizing treatment. After removing the lowest 1.1% elongation and 746 MPa tensile strength values, which are considered unrepresentative due to the sample's defects, the mechanical properties for the intercritical (IC) austenitizing treatment was one 3-sample dataset and the mechanical properties for the supercritical (SC) austenitizing treatment was the second 4-sample dataset. The means and standard deviations were calculated for these two sets of data. The results are shown in Table 6.

Microsoft Excel® was also used to conduct 2-sample and two-tailed F-testing, which is a hypothesis test for two sample variances to determine whether they are significantly different.[23] This test was performed to determine whether Student's t-testing should be performed with equal or unequal variances. This procedure uses a null hypothesis that the difference between two population variances ($\sigma2$), or the square of the standard deviation (σ), is equal to a hypothesized (H) value (H0: $\sigma12 - \sigma22 = 0$ or $\sigma_1^2 = \sigma_2^2$) and tests it against an alternative hypothesis (H1: $\sigma_1^2 \neq \sigma_2^2$).

One result of the F-test is the value "P". The rejection probability (P), also called alpha (α), was measured for each of the dependent variables versus heat treatment method in the F-tests. P ranges from 0 to 1. In a one-tailed test, P would be 0.05. However, in two-tailed F-tests with
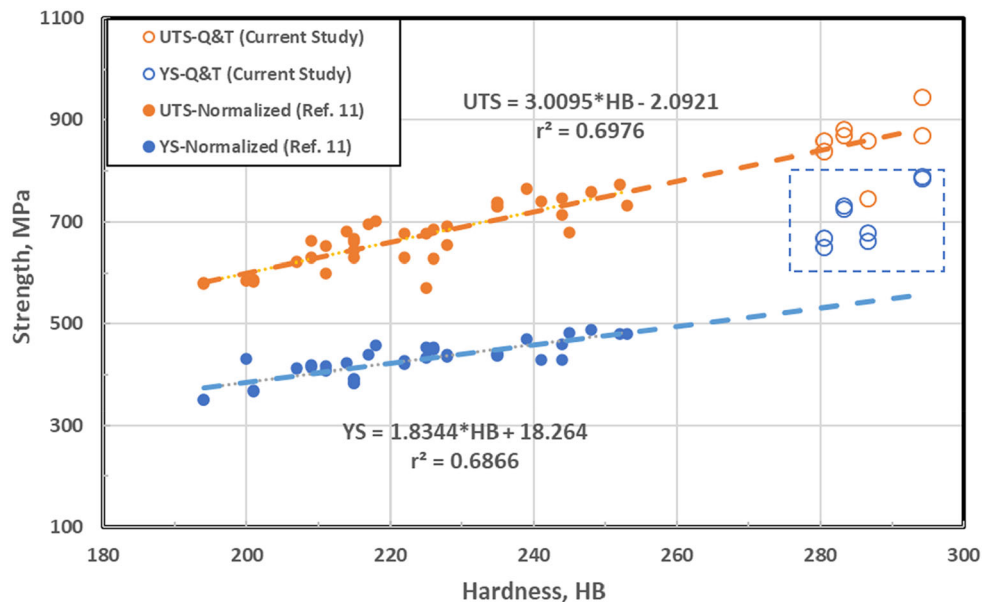

Figure 9. The correlation of hardness with strength is shown for the Q&T alloys (open points) of this study as compared to the normalized (air-cooled) acicular pearlite + ferrite structures of a previous study.[11] All materials were cooled from an intercritical temperature.

Table 6. Statistics for Selected Mechanical Properties

Property	0.2% Offset yield strength (YS)		Ultimate tensile strength (UTS)		Elongation (El)		Toughness (U_T)	
Units	MPa		MPa		%		MPa-mm/mm	
Austenitizing Treatment	IC	SC	IC	SC	IC	SC	IC	SC
Averages	665	759	853	893	4.9	3.3	37.5	26.8
Standard Deviations	12	34	12	36	0.5	1.3	4.1	10.6
F-test, rejection probability (P)	0.059		0.103		0.121		0.134	
t-test, significance probability (1−P)	99.8%		88.9%		93.0%		86.0%	

the SC treatment results being population 1 because they had the larger variance, the comparison P was set to 0.1.[23] As shown in Table 6, all rejection probabilities F-tests were greater than 0.1 except for the YS comparison. Therefore, equal variance was used for the YS comparison in the Student's t-testing, but unequal variance was used for comparing the three other properties (UTS, El, and U_T).

Microsoft Excel® was also used to conduct 2-sample and two-tailed Student's t-testing, which is a hypothesis test for two small sample means with unequal variances to determine whether they are significantly different.[23] This test essentially determines whether or not there are significant differences between two sets of data.

This procedure uses the null hypothesis that the difference between two population means (μ) is equal to a hypothesized (H) value (H_0: $\mu_1 - \mu_2 = 0$ or $\mu_1 = \mu_2$) and tests it against an alternative hypothesis (H_1: $\mu_1 \neq \mu_2$).[23] As with the F-test, a result of the t-test is the value "P". The rejection probability (P), also called alpha (α), was measured for each of the dependent mechanical property variables versus heat treatment type (IC and SC) in the t-tests. P ranges from 0 to 1.

The smaller the P-value, the smaller the probability that rejecting the null hypothesis is a mistake. The P-value is calculated from the observed sample and represents the probability of incorrectly rejecting the null hypothesis when it is actually true (Type 1 error). In other words, it is the probability of obtaining a difference at least as large as the one between the observed value and the hypothesized value through random error alone.

After multiplying the P-value by 100 to convert it to a percentage, 100 minus the P% gives the "percent confidence" about stating that the IC austenitizing property differs significantly from the SC austenitizing property. If

the test's P-value is less than some chosen level (usually 0.05 or 5%), then H_0 should be rejected and H_1 accepted.

The Student's t-value confidence probabilities are shown in Table 6. The t-test averages showed that the IC austenitizing treatment produced yield and tensile strengths that were lower, and ductility and toughness values that were higher, than the comparable values produced by the SC austenitizing treatment. The differences in YS values are highly significant with greater than 99.8% confidence, i.e., rejection $P < 5\%$. Although the differences in UTS, ductility and toughness values between the two heat treatments were less significant, with confidence probabilities ranging from 86 to 93% confidence (P ranging from 14 to 7%), considering the small sample sizes, even these differences are very convincing.

Metallography and Microstructure

Metallographic samples were cut from selected broken tensile specimens on a band saw. All samples were compression-mounted in Bakelite, then ground, polished, and Nital-etched in accordance with ASTM E311(2017). Optical micrographs were obtained from selected samples.

Selected samples were also placed in a scanning electron microscope (SEM) for further documentation at magnifications between 100 to 5000X, at a working distance of 15 mm, and an accelerating voltage of 20 kV. Both secondary electron (SE) and back-scattered electron (BSE) micrographs were obtained from the following conditions:

1. Alloy 1, as-cast
2. Alloy 3, as-cast
3. Alloy 1, supercritically austenitized, quenched and tempered at 538°C (1000°F) for 8 hours

4. Alloy 3, intercritically austenitized, quenched and tempered at 538°C (1000°F) for 4 hours

The SE images provide topographic contrast, whereas darker regions in the BSE images represent regions containing elements that have lower atomic numbers and weights.

Bombardment with electrons nondestructively created X-rays that are characteristic of the various elements on the surfaces of the samples. The X-rays were dispersed with respect to their characteristic energies to determine the elemental content using energy dispersive spectroscopy (EDS).

Atmospheric thin-window EDS mode was employed with the microscope operated at 20 kV accelerating voltage. In this mode, the EDS system can identify elements with atomic number (Z) greater than or equal to 5 (boron). EDS cannot accurately quantify the contents of light elements such as carbon and oxygen, but they can be qualitatively compared.

To provide greater detail beyond the optical image in Figures 7 and 10 illustrates the as-cast mostly pearlitic microstructures in Alloys 1 and 3.

Figure 11 illustrates the microstructures of an IC heat-treated sample of Alloy 3. The grain structure of martensite and ferrite is visible in all the figures. Figure 11b shows that the interdendritic (cell) boundaries contain some shrinkage porosity and are mostly martensitic, whereas the cell interiors have a mixture of lamellar grain morphology with both martensite and ferrite grains. Figure 11f contains mostly lath martensite.

Figure 12 shows the microstructures in an SC heat-treated sample of Alloy 1. The martensitic microstructure has mostly equiaxed grain morphology. Figure 12d shows both lath and plate martensite.

The carbon content dissolved in the austenite component was determined according to the formulae reported by Nieswaag and Nijhof[24] for Fe-Si-C alloys. For supercritical heat treatment at 899 °C (1650 °F), an austenite with 2.4%Si contains 0.87%C. At the upper critical temperature, nominally 800 °C (1472 °F), austenite dissolves 0.61%C. In the intercritical region, the austenite component dissolves even less than 0.61%C. According to Krauss,[25] plate martensite forms when carbon contents exceed 0.6%. Therefore, some plate martensite is expected in the supercritically heat-treated material (with 0.87%C based on our estimates), but not necessarily with the intercritically austenitized material (with <0.61%C).
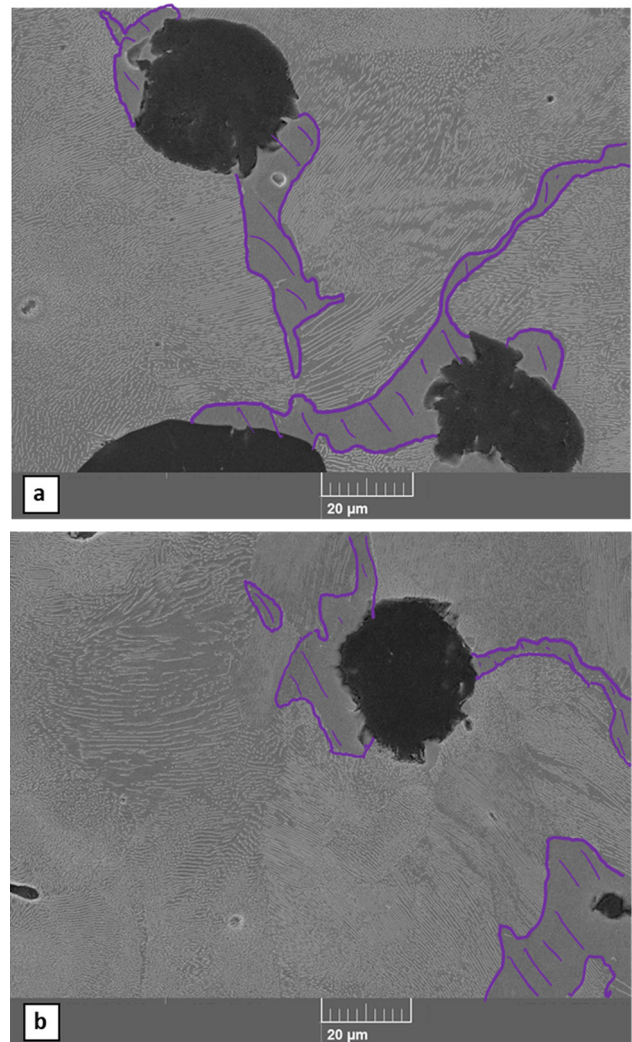

Figure 10. SEM micrographs of the etched pearlite microstructures of (a) Alloy 1 and (b) Alloy 3 are shown in the as-cast condition at the same magnification. The black circular particles are graphite and the outlined regions are ferrite. All the rest of the matrix structure is pearlite. Etched in 2% Nital.

Secondary Graphite or Temper Carbon Formation

The samples of the supercritically heat-treated materials displayed small dark particles of secondary graphite, as shown in Figures 12c, d and 13. Although carbon and oxygen contents can only be compared qualitatively, the EDS probes summarized in Table 7 show that the particles contain higher carbon contents and oxygen, as compared to the matrix. This secondary graphite formed during tempering and is also called "temper carbon." It is well known that secondary graphite forms during the tempering of Q&T martensitic DI and generally occurs only when
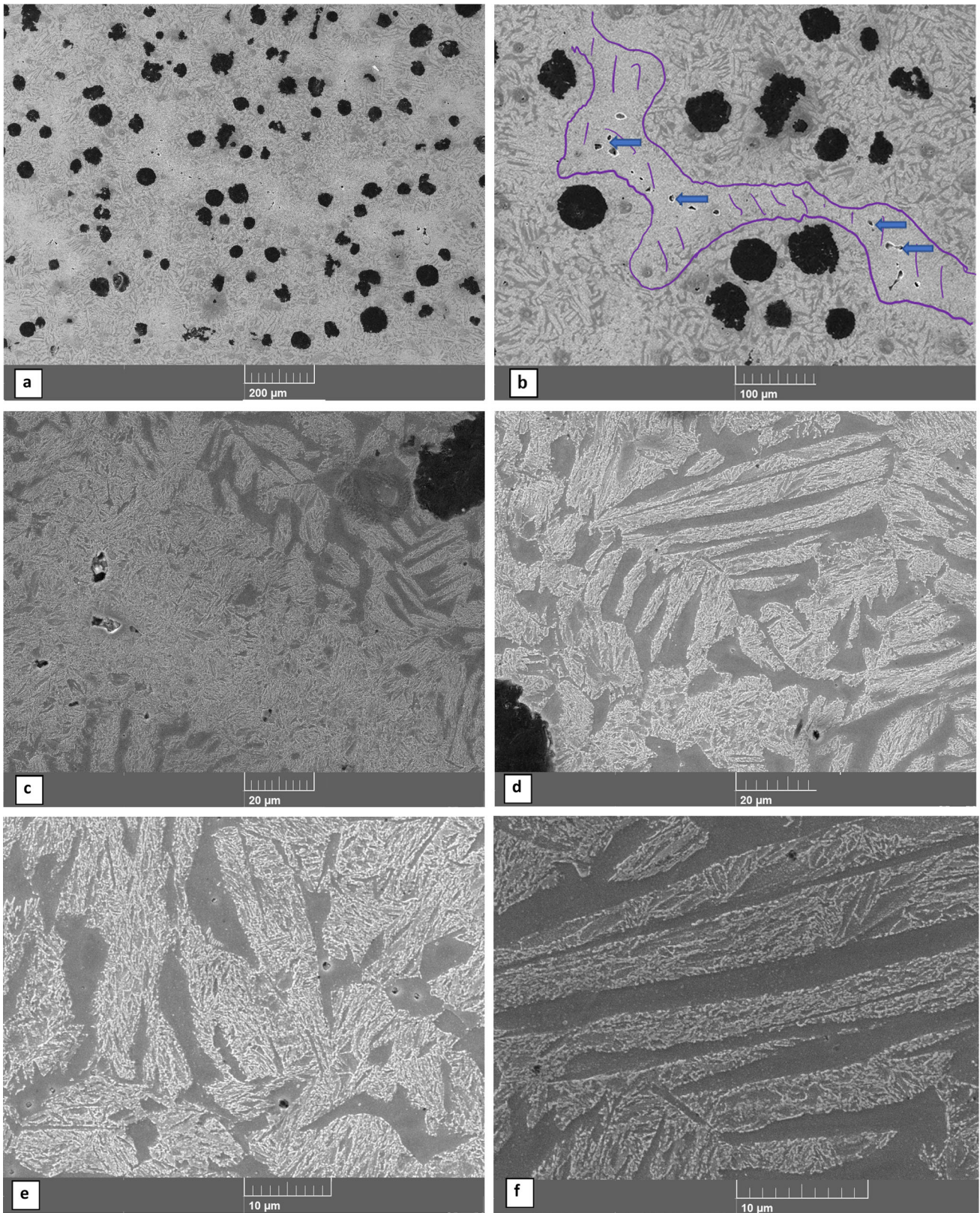
Figure 11. *SE micrographs of intercritically austenitized Alloy 3 at increasing original magnifications of (a) 200X, (b) 500X, (c) 2000X, (d) 3000X, (e) 5000X, and (f) 7500X. Selected interdendritic regions are outlined in purple, and blue arrows indicate porosity in (b). Etched in 2% Nital.*
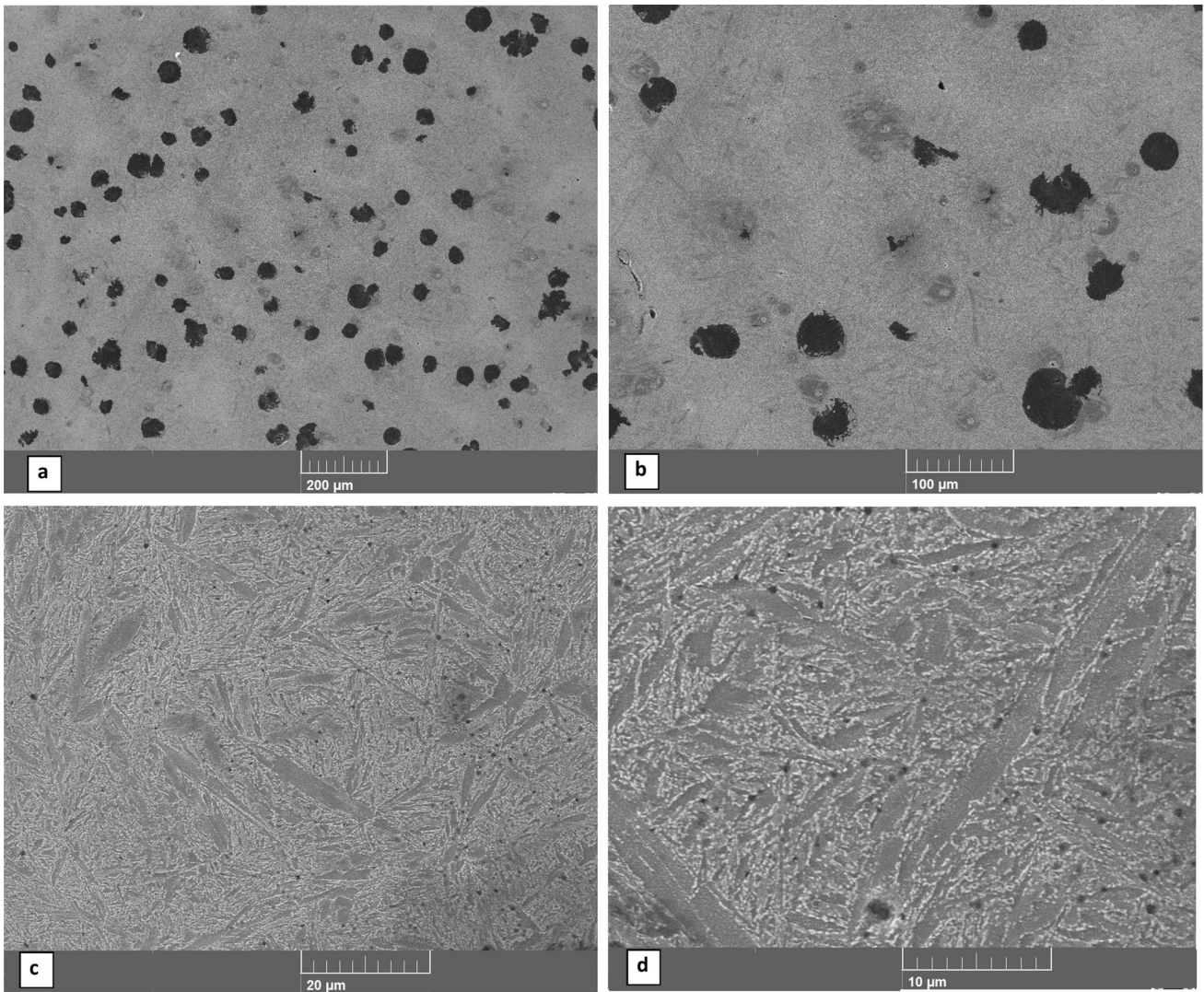
Figure 12. SE micrographs of supercritically austenitized Alloy 1 at increasing original magnifications of (a) 200X, (b) 500X, (c) 3000X, and (d) 7000X. Etched in 2% Nital.
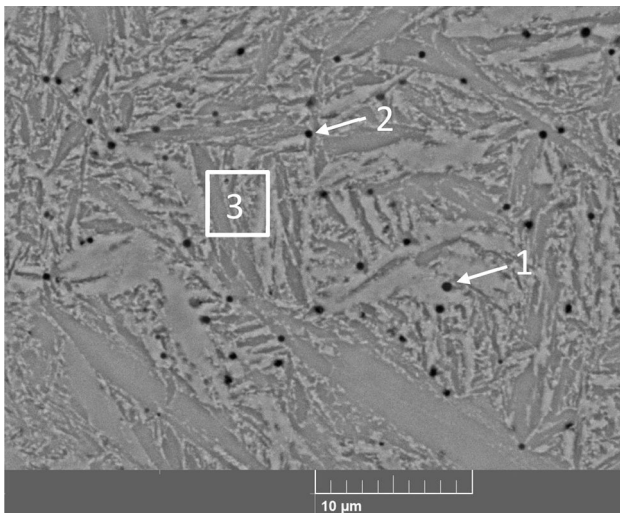

Figure 13. BSE micrograph of supercritically austenitized Alloy 1 in a similar region to Figure 12d. Etched in 2% Nital.

Table 7. Semiquantitative EDS Analysis (in wt%) in Three Locations in Figure 13

Element	Spot #1 Temper carbon	Spot #2 Temper carbon	Box #3 Matrix
C	13	11	4.6
O	0.55	1.5	–
Si	0.91	1.5	1.1
Mn	0.42	0.76	0.82
Cu	0.52	–	0.68
Fe	Bal.	Bal.	Bal.

heating above 482 °C (900 °F).[26] Since tempering was performed at 540 °C (1000 °F), it is not surprising to see secondary graphite in the supercritically heat-treated materials. No temper carbon was observed in the inter-critically heat-treated materials, see Figure 12. Similar findings were reported earlier,[12] where Q&T martensitic

ductile iron displayed temper carbon, whereas IC heat-treated ductile iron did not.

It is noteworthy that secondary graphite was not observed in the intercritically heat-treated materials which were also quenched and tempered at the same tempering temperature. As discussed earlier,[26] perhaps the lower-carbon martensite in the IC heat-treated material is less susceptible to decomposition and the formation of secondary graphite.

Discussion

The principal objective of this investigation was to determine whether intercritical (IC) heat treatment can improve the strength and ductility of Q&T ductile iron. IC heat treatment produced a unique lamellar structure consisting of acicular martensite in ferrite. The microstructures showed that numerous discrete acicular austenite grains nucleate and grow from the ferrite grain boundaries and result in the formation of a microstructure consisting of "lamellar" austenite in ferrite.

The high strength and ductility observed in the test specimens is attributed to the fine-grained lamellar martensite + ferrite structure that forms on quenching from the intercritical temperature, as shown in Figure 14. This micrograph shows that intercritical austenitizing near the upper critical temperature can form a high density of austenite needles inside one single ferrite grain.

The tensile properties of ductile iron are a function of both matrix microstructure and graphite nodule characteristics. Table 2 shows that the experimental alloys have relatively low nodule counts with some very coarse graphite nodules, because they are thick section castings. Note that, unlike the ISO 1083 standard, ASTM A536 makes no allowance for the loss in ductility in heavy-section castings. When the properties are compared to the Q&T grades of EN 1563 and ISO 1083, the IC heat-treated alloys display significantly higher ductility; they might have exhibited even better strength-toughness combinations, if they had been cast in thinner sections.

Transformation Behavior

Ductile iron produces a unique lamellar microstructure during intercritical heat treatment. This novel lamellar austenite+ ferrite structure provided a unique approach to austenite grain refinement, and it was applied to quench and temper ductile iron in order to improve the strength-ductility properties. Compared to the coarse-grained, polygonal austenite that forms on heating above the upper critical temperature, the lamellar austenite structures can be an order of magnitude finer. Figure 15 shows a schematic of how this novel microstructure forms in ductile iron.

In ductile iron, the isolation of the carbon phase affects the kinetics of phase transformation in heat treatment. On heating above the lower critical temperature, multiple acicular austenite grains nucleate at the ferrite grain boundaries and grow into the ferrite grains. Since the ferrite grains are isolated from the carbon source (graphite nodules), carbon enters the ferrite grain at the grain boundaries only, as long as pearlite is absent prior to intercritical austenitizing. (If pearlite is present, the carbon is already present in the cementite, and there is no need to obtain carbon from the graphite.) Carbon flow into the ferrite grain is limited by the transport of carbon across the graphite-matrix interface. Transport is slow, as the interface between the graphite nodule and matrix is not fully coherent. During intercritical austenitizing, coherency is
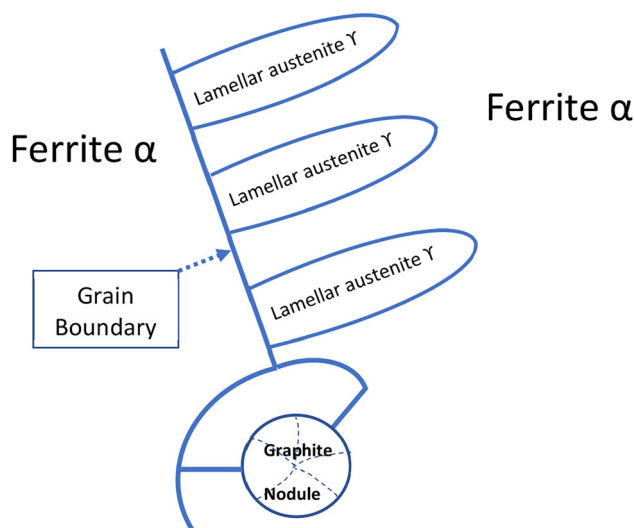

Figure 14. Optical micrograph showing quenched microstructure illustrating the unique lamellar austenite in ferrite structure that had formed by intercritical heat treatment.

Figure 15. Schematic illustrating the formation of lamellar austenite by intercritical (IC) austenitizing of ferritized ductile iron.

reduced by the consumption of carbon from the graphite nodules and their separating away from the matrix during recarburization of the matrix. Furthermore, the authors opine that the graphite that formed during solid state graphitization (occurring during cooling from the eutectic to the eutectoid temperature) is less dense.[27] The slow recarburization of the ductile iron matrix on heat treatment is well-documented.[20] To reach equilibrium at the inter-critical austenitizing temperature, our experiments show a minimum soak time of 2 hours is recommended.

The lamellar austenite + ferrite structure forms in packets within the ferrite grains. As shown in Figure 1a, these packets of lamellar austenite + ferrite form inside the ferrite grains of IC heat-treated materials just like packets of lath martensite form inside prior austenite grains for SC heat-treated materials. The microstructures of IC heat-treated samples contained significant amounts of ferrite. As in austempered ductile iron, it was anticipated that the finely distributed ferrite would enhance ductility and toughness.

Segregation

It is well known that the solute elements segregate/partition between the growing solid phase and the remaining liquid metal during solidification. Numerous investigators have documented the segregation of the common elements used in ductile iron. In his classic paper, Rundman summarizes the segregation behavior.[28]

Recognizing that in DI, the metallic phase (austenite) grows dendritically, alloying elements will either partition to the cores of the dendrites, or to the interdendritic regions. Since each alloying element has a unique influence on the UCT and carbon activity in austenite, alloy segregation is expected to modify the UCT from location to location. Researchers[19] have shown that, of the common alloying elements, Si and Mn have the greatest influence on UCT. They also showed that their effects are opposite; Si raises UCT and Mn lowers it. Si also segregates negatively (to the first solid to form), and Mn segregates positively (to the last metal to freeze).

Consequently, the UCT in the core of the dendrites is above that in the interdendritic region. The effects of segregation are quite evident in the distribution of ferrite in the intercritically heat-treated materials. The micrograph in Figure 11b shows that the ferrite is confined to the dendrite cores and the interdendritic regions are devoid of ferrite.

Energy-dispersive spectrometry was performed on the as-cast sample from Alloy 3. Areas from both the core region and interdendritic region were probed to document differences in elemental content due to alloy segregation during solidification. Figure 16 shows companion high-
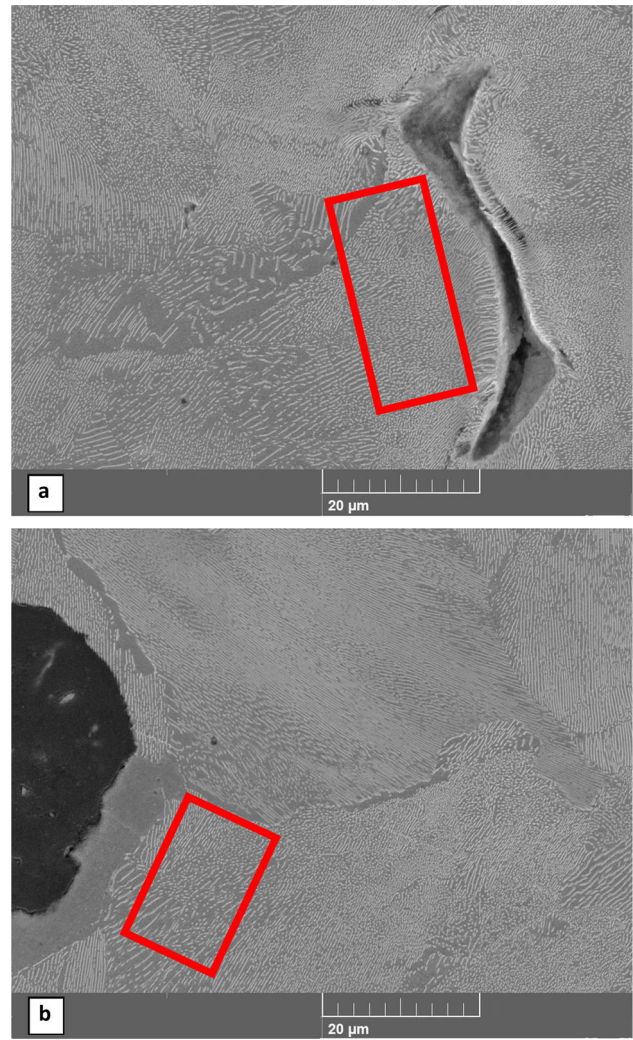

Figure 16. SEM views in as-cast Alloy 3. (a) SE micrograph in interdendritic region with solidification pore (b) SE micrograph in pearlite adjacent to a graphite nodule in the dendrite core region. Etched in 2% Nital.

Table 8. Semiquantitative EDS Analysis and Calculated UCT in Two Locations in Figure 16

Quantity	Unit	Figure 16a Interdendritic region	Figure 16b Dendrite core region
Si	wt%	1.81	2.29
Mn		0.29	0.25
Ni		0.40	0.46
Cu		0.09	0.37
UCT	°C(°F)	815 (1498)	837 (1539)

magnification SEM micrographs, and Table 8 shows the corresponding semiquantitative EDS analyses in both the dendrite core and interdendritic regions.

Using the formulae of Reference 18, as well as the Si and Mn concentrations of the core, Table 8 shows the UCT values that were determined for both the core and
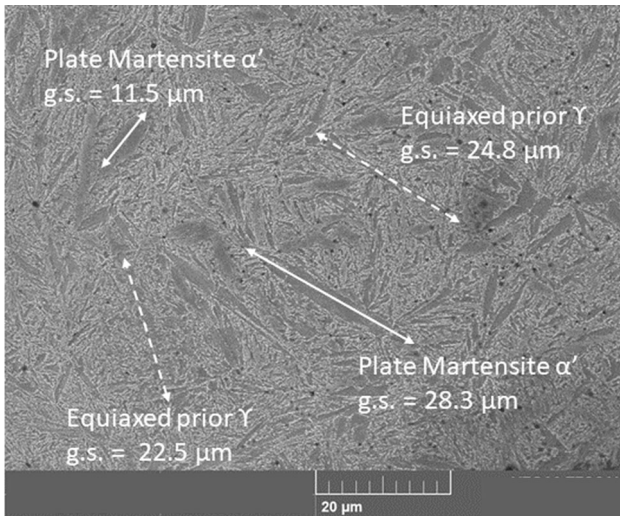
Figure 17. SE micrograph with grain size measurement in plate martensite (α′) and prior austenite (γ) grains of supercritically austenitized and tempered sample of Alloy 1. Etched in 2% Nital.

interdendritic regions. Due to segregation, Table 8 shows that the difference in UCT is roughly 22 °C (41 °F).

Grain Refinement

The martensite constituents consisted of both lath and plate martensite forms. Both are expected for austenite carbon levels of 0.6 to 1.0%C according to Krauss.[25] For the supercritically heat-treated materials, where austenite carbon levels are predicted to be greater than 0.8%C, significant amounts of plate martensite were observed. Since plate martensite typically nucleates on the austenite grain boundary and traverses the grain, the size/length of the plate martensite needles reflects the size of the austenite grains. Plate martensite needles are shown in Figure 17 and range in size from 11 to 28 um.

Alternately, Figure 18 shows that the acicular austenite grains in the intercritically heat-treated materials displayed lengths of 16 to 24 um and widths of 4 to 6 um.

In the interdendritic region, the microstructure is largely martensitic. In the dendrite core region, it is lamellar martensite in ferrite. This is due to the difference in upper critical temperature of the two regions as discussed above with respect to Figure 16. This is also the reason why there is a grain morphology change. There is a finer grain size in the interdendritic region of the IC heat-treated material versus SC material (compare Figures 18a and 17, respectively). The equiaxed austenite grain size in the SC material is coarser with 22.5 and 24.8 um (in Figure 17) versus the interdendritic region of the IC material with austenite grain size 9.4 and 11.2 um (in Figure 18a). This is primarily due to the difference of austenitizing temperature
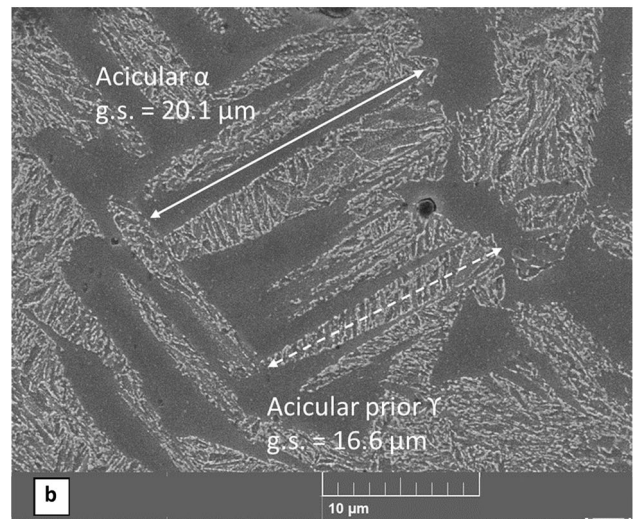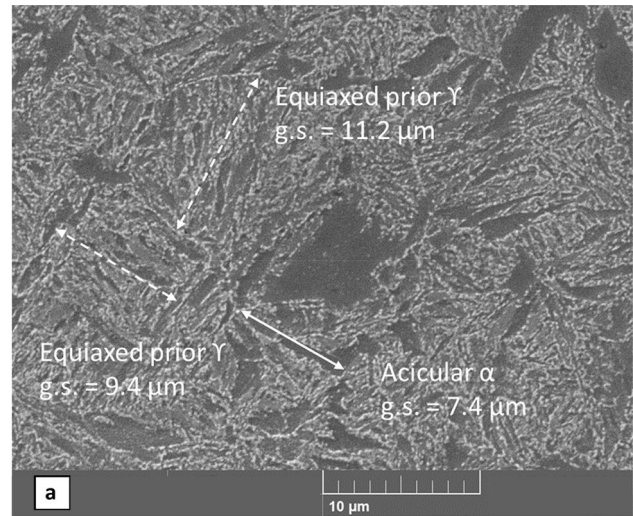

Figure 18. SE micrographs of microstructure with grain size measurements of prior austenite (γ) grains in ferrite (α) of intercritically austenitized and tempered sample of Alloy 3. View (a) of equiaxed grains in the interdendritic region and view (b) of acicular grains in the lamellar region in dendritic core. Etched in 2% Nital.

[827 °C(1520 °F) for the IC austenitizing versus 899 °C (1650 °F) for the SC austenitizing]. For the dendritic core of the IC material, there is a change in morphology to a lamellar structure where long (20.1 um) and thin (2 to 4 um) austenite grains transform to long and thin acicular martensite, which is also a form of grain refinement.

Conclusions

This study utilized quenching from an intercritical temperature, near the upper critical temperature (in contrast to earlier investigators who austenitized at lower intercritical temperatures). Thus, this study produced a unique microstructure consisting of lamellar martensite in ferrite. This transformation structure is unique to ductile iron (and possibly to other graphitic cast irons). Intercritical heating

near the upper critical temperature produced a structure of acicular austenite in ferrite which, upon quenching, transformed to martensite, producing a fine-grained acicular structure. After tempering, the mechanical properties exceed the properties of the Q&T grades of the ASTM A536 and ISO 1083 specifications. The test results of this study demonstrated that quenching from an intercritical temperature will produce high ductility at specified strength in the quenched and tempered grades of ductile iron.

For the investigation, intercritical (IC) heat treatment and comparison with supercritical (SC) heat treatment of two ductile iron alloys were performed. The results of mechanical testing and microstructure evaluations showed the following:

1. A unique lamellar martensite + ferrite structure was achieved by intercritical heat treatment. With widths of 4 to 6 um and lengths of 16 to 24 um, the austenite grain size was substantially finer than the polygonal austenite grain structure with diameters of 11 to 28 um produced by conventional hardening above the critical temperature.
2. Due to segregation, higher Si and lower Mn contents were measured in the dendrite core versus the interdendritic region of an as-cast ductile iron.
3. Intercritical heat treatment was performed at a temperature where a fine-grained lamellar austenite + ferrite formed in the core region without forming a continuous network of austenite in the interdendritic regions.
4. Ferritization annealing prior to heating in the IC temperature region produced a more uniform distribution of lamellar austenite in ferrite as compared to IC heat treatment of ductile iron with mixed structures of ferrite and pearlite.
5. When the properties are compared to the minimum specifications for the Q&T grades of ASTM A536 Grade 120-90-02 and ISO 1083 Grade 900-2, the experimental alloys exhibited the specified tensile properties. The IC heat-treated grades had up to 5% tensile elongation, which was higher than the standard grades with 2% elongation.
6. Statistical tests confirmed that the IC heat-treated grades had somewhat lower yield and tensile strengths, but higher ductility and tensile toughness than the SC grades.
7. The best combination of strength and toughness was obtained by intercritically austenitizing Alloy 1 containing 3.6C-2.3Si-0.3Mn-0.6Cu-0.24Ni. The alloy was austenitized at 832 °C (1530 °F) for 4 hours and tempered at 538 °C (1000 °F) for 4 hours to a hardness of 280 HB. Average values of yield strength of 662 MPa (96 ksi), tensile strength of 848 MPa (123 ksi), and elongation of 4.8% were obtained. If a thinner section had been cast, it is possible that even better tensile properties would have been obtained.
8. The tempering of supercritically heat-treated martensitic structures produced secondary graphite or temper carbon, whereas none was observed in the intercritically heat-treated materials on tempering up to 540 °C (1000 °F).

Acknowledgements

REFERENCES

1. Y. Tomita and K. Okabayashi, "Effect of Microstructure on Strength and Toughness of Heat-treated Low Alloy Structural Steels," Met Trans. A, 17A, 1986
2. R. Cryderman, Metallurgical strategies for higher strength induction hardened parts: induction hardening parts with small grain size achieves higher fracture strengths, but close control of thermal cycles is required to prevent grain growth. Adv. Mater. Process. ASM Int. **177**(8), 63 (2019)
3. X. Li, X. Ma, S.V. Subramanian, S. Shang, R.D.K. Misra, Influence of prior austenite grain size on Martensite-Austenite constituent and toughness in the heat affected zone of 700 MPa high strength linepipe steel. Mater. Sci. Eng. A **616**(20), 141 (2014)
4. S. Morito, H. Yoshida, T. Maki, X. Huang, Effect of block size on the strength of lath martensite in low carbon steels. Mater. Sci. Eng. A **438–440**, 237 (2006)
5. B. Bialobrzeska, L. Konat, R. Jasinski, The influence of austenite grain size on the mechanical properties of low-alloy steel with boron. Metals **7**(26), 1 (2017). https://doi.org/10.3390/met7010026
6. F. Zanardi, "The Development of ADI and IDI in Italy" AFS/DIS 2008 Keith Millis Symposium on Ductile Cast Iron, 2008
7. W.L. Guesser, C.L. Lopes, P.A.N. Bernardini, Austempered ductile iron with dual microstructures: effect of initial microstructure on the austenitizing process. Inter. Metalcast. **14**, 717–727 (2020). https://doi.org/10.1007/s40962-019-00397-y
8. R. Aristizabal, R. Foley, A. Druschitz, Intercritically austenitized quenched and tempered ductile iron. Inter. Metalcast. **6**, 7–14 (2012). https://doi.org/10.1007/BF03355534
9. M. Lagarde, A. Basso, R.C. Dommarco, J. Sikora, Development and characterization of a new type of

ductile iron with a novel multi-phase microstructure. ISIJ Int. **51**(5), 645–650 (2011)

10. J.M. Tartaglia, R.B. Gundlach, G.M. Goodrich, Optimizing structure-property relationships in ductile iron. Inter. Metalcast. **8**, 7–38 (2014). https://doi.org/10.1007/BF03355592

11. R.B. Gundlach, *"Normalizing Heat Treatments to Develop Improved Properties in Heavy-Section Ductile Iron", Report for Research Project 48* (Ductile Iron Society, Strongsville, OH, 2014)

12. H.D. Machado, R. Aristizabal, C. Garcia-Mateo, I. Toda-Caraballo, Effect of the starting microstructure in the formation of austenite at the intercritical range in ductile iron alloyed with nickel and copper. Inter. Metalcast. **14**, 836–845 (2020). https://doi.org/10.1007/s40962-020-00450-1

13. R. Aristizabal, K. Hayrynen, R. Foley, J. Griffin, C. Monroe, Austemperability of intercritically austempered ductile iron. AFS Trans. **112**, 279–286 (2014)

14. R.B. Gundlach, *"Achieving Higher Strength and Toughness in Heavy-Section Ductile Iron Castings", Report for Research Project 63* (Ductile Iron Society, Strongsville, OH, 2021)

15. R. B. Gundlach and J. M. Tartaglia, "A Novel Approach to Austenite Grain Refinement," AFS Trans. **130**. pp tbd (2022), to be published

16. ASTM Standard A536, Spheroidal Graphite Cast Irons, ASTM, 2018

17. International Standard ISO 1083, Spheroidal Graphite Cast Irons—Classification, International Organization for Standardization, 2004.

18. E. Piwowarsky, *Hochwertiger Gusseisen*, 2nd edn. (Springer Verlag, Berlin, 1958)

19. K.L. Hayrynen, J.R. Keough, B.V. Kovacs, *"The Effects of Alloying Elements on the Critical Temperatures in Ductile Iron", Ductile Iron Society, Report for Research Project 22* (Ductile Iron Society, Strongsville, OH, 1997)

20. J. Lincoln, "ADI-Commercial Applications and Facilities," 2nd International Conference on Austempered Ductile-Your means to improved Performance, Productivity and Cost," ASME, Ann Arbor, MI, USA, March 17-19, 1986

21. R. E. Savage, "Heat Treating Ductile Iron," *Steel*, vol. 137, 1975

22. G.E. Dieter, *Mechanical Metallurgy*, 3rd edn. (McGraw Hill, New York, 1986)

23. W. Mendenhall and J. E Reinmuth, "Statistics for Management and Economics, Second Edition, Duxbury Press, 1974, pp. 220-225 and 234-236, and https://www.lifewire.com/how-to-do-a-t-test-excel-4689479

24. H. Nieswaag and J. W. Nijhof, "Influence of Silicon on Bainite Transformation in Ductile Iron; Relation to Mechanical Properties," The Physical Metallurgy of Cast Irons, Proceedings of the Third International Symposium on the Physical Metallurgy of Cast Iron, Stockholm, Sweden, Aug. 29-31, 1984, Materials Research Society, pp. 411-422

25. G. Krauss, "Steels-Processing, Structure, and Performance," ASM International, 2005, p. 71

26. D. R. Askeland and N. Birer, "Secondary Graphite Formation in Tempered Nodular Cast Iron Weldments," Welding Research Supplement, pp. 337s-342s, 1979

27. P. Rubin, R. Larker, E. Navara, M.-L. Antti, Graphite formation and dissolution in ductile irons and steels having high silicon contents: solid-state transformations. Metallogr. Microstruct. Anal. **7**, 587–595 (2018). https://doi.org/10.1007/s13632-018-0478-6

28. K. B. Rundman, "Controlling the Segregation of Alloying Elements in Austempered Ductile Iron," An AFS Special Report, American Foundrymen's Society, 1998